

SYNTHESIS OF POLYCRYSTALLINE METHANE HYDRATE, AND ITS PHASE STABILITY AND MECHANICAL PROPERTIES AT ELEVATED PRESSURE

Laura A. Stern, Stephen H. Kirby (both at: USGS, Menlo Park, CA 94025)
and William B. Durham (UCLLNL, Livermore, California, 94550)

Key words: gas hydrate synthesis; reaction kinetics; mechanical properties

Abstract

Test specimens of methane hydrate were grown under static conditions by combining cold, pressurized CH_4 gas with H_2O ice grains, then warming the system to promote the reaction $\text{CH}_4(\text{g}) + 6\text{H}_2\text{O}(\text{s}) \rightarrow \text{CH}_4 \cdot 6\text{H}_2\text{O}$. Hydrate formation evidently occurs at the nascent ice/liquid water interface, and complete reaction was achieved by warming the system above 271.5 K and up to 289 K, at 25-30 MPa, for approximately 8 hours. The resulting material is pure methane hydrate with controlled grain size and random texture. Fabrication conditions placed the H_2O ice well above its melting temperature before reaction completed, yet samples and run records showed no evidence for bulk melting of the ice grains. Control experiments using Ne, a non-hydrate-forming gas, verified that under otherwise identical conditions, the pressure reduction and latent heat associated with ice melting is easily detectable in our fabrication apparatus. These results suggest that under hydrate-forming conditions, H_2O ice can persist metastably at temperatures well above its melting point.

Methane hydrate samples were then tested in constant-strain-rate deformation experiments at $T = 140\text{--}200\text{ K}$, $P_c = 50\text{--}100\text{ MPa}$, and $\dot{\epsilon} = 10^{-4}\text{--}10^{-6}\text{ s}^{-1}$. Measurements in both the brittle and ductile fields showed that methane hydrate has measurably different strength than H_2O ice, and work hardens to a higher degree compared to other ices as well as to most metals and ceramics at high homologous temperatures. This work hardening may be related to a changing stoichiometry under pressure during plastic deformation; x-ray analyses showed that methane hydrate undergoes a process of solid-state disproportionation or exsolution during deformation at conditions well within its conventional stability field.

INTRODUCTION

Methane hydrate is a nonstoichiometric compound consisting of a network of H_2O molecules that are hydrogen-bonded in a manner similar to ice and interstitially encaging CH_4 gas molecules (1). Distributed globally in shallow marine and permafrost environments, methane hydrate harbors a significant yet virtually untapped hydrocarbon source (2,3,4). Despite scientific interest in this compound and potential commercial importance, many of the physical and material properties of methane hydrate are as yet poorly constrained or unmeasured, and a full understanding of these properties will eventually be needed to turn potential energy projections into practical plans for its recovery. We have now established optimal growth parameters for efficient synthesis of methane hydrate suitable for such testing, and have measured these samples in deformation experiments to determine fracture and flow characteristics. The results revealed some anomalous behavior in the formation, plastic flow behavior, and stability of methane hydrate at elevated pressure (5).

SAMPLE SYNTHESIS

Our objective was to synthesize large-volume, cohesive, low-porosity, polycrystalline hydrate aggregates with controlled, fine grain size and random crystallographic grain orientation. Our technique differs from previous studies (6), most of which involve continuous agitation of reaction mixtures, resulting in strongly textured material unsuitable for materials testing. We produced samples of virtually pure methane hydrate by the general reaction $\text{CH}_4(\text{g}) + 6\text{H}_2\text{O}(\text{s}) \rightarrow \text{CH}_4 \cdot 6\text{H}_2\text{O}(\text{s})$, by the mixing and subsequent slow, regulated heating of sieved granular ice and cold, pressurized CH_4 gas in an approximately constant-volume reaction vessel (Figs. 1, 2, & 3A).

Sample fabrication details are as follows: CH_4 gas from a source bottle is initially boosted in pressure (P) by a gas intensifier and routed into sample molding vessels housed in a deep freezer. The sample assembly (Fig. 2) consists of two steel vessels immersed in an ethyl alcohol bath initially held at freezer temperature (T) of 250 K. One vessel serves as a reservoir to store and chill pressurized CH_4 gas, and the other houses the sample mold. The mold consists of a hollow split-cylinder that encases an indium sleeve filled with 26 g of H_2O ice "seed" grains, packed to 40% porosity. Seed material is made from a virtually gas-free, single-crystal block of triply distilled H_2O ice, ground and sieved to 180-250 μm grain size. Initially, the sample chamber with seed ice is closed off from the reservoir and is evacuated. A loosely fitting top disk inserted on top of the packed seed ice grains (Fig. 2) prevents displacement of the packed ice grains during evacuation.

The reservoir vessel is first charged with pressurized CH_4 gas to 34 MPa, and cools to 250 K. The reservoir is then opened to the pre-evacuated sample chamber, and CH_4 pressure drops to roughly 22 MPa. These steps serve to fill the porosity between the ice grains at a molar ratio of CH_4 to H_2O in the sample vessel well in excess of that required for full hydrate formation (7, 8). The bath T is then slowly raised by means of the hot plate situated beneath the alcohol bath (Fig. 2). As the sample and reservoir warm, they self-pressurize. Pressure increases steadily with increasing T until reaction initiates, at which point consumption of CH_4 gas by hydrate formation slows the rate of P increase. Data-acquisition software (LabVIEW, National Instruments) was used to monitor and record P and T conditions throughout each run, and the extent of reaction was determined by the measured P_{CH_4} offset from the reversible CH_4 expansion curve.

Following full reaction, the heat source is turned off and the system slowly cools back down to 250 K. The sample chamber is then quenched in liquid nitrogen, isolated from the reservoir, vented, disconnected from the apparatus, and opened. The inner, hollow split-cylinder containing the sample is pushed from the mold and pried off the jacketed sample. Samples are then stored in liquid nitrogen until mechanical testing.

THE HYDRATE-FORMING REACTION & POSSIBLE SUPERHEATED ICE

Representative pressure-temperature (P-T) and temperature-time (T-t) histories during a reaction run are shown in Figure 4. Up to at least 271.5 K, CH₄ pressure increases approximately linearly with T with a slope largely governed by the equilibrium thermal expansion of free CH₄ in the reservoir and sample reaction vessel. Progress of the hydrate-forming reaction was monitored by observing the deflection of P from this linear P-T curve, a deflection that accompanies the volume reduction associated with reaction. Completion of the reaction is marked by a P offset (ΔP_r) of 1.8 ± 0.1 MPa at a peak T of ~ 289 K, a state that is reached over a heating time interval of about 8 hours after the vessel crosses the 271.5 K isotherm (Fig. 4). After cooling to 77 K while venting unreacted CH₄, the resulting samples were shown by x-ray diffraction measurements to be virtually pure methane hydrate, with minor amounts of ice (0-3%) being the only additional phase (Fig. 3). That practically all the H₂O reacted to form hydrate was also consistent with both the calculated molar volume reduction of the reaction (9), and with the lack of a P-T anomaly associated with freezing of unreacted liquid water (Fig. 4A, cooling curve). Measurements of the mass uptake of CH₄ in fully reacted samples also were consistent with essentially complete reaction of the original H₂O to form hydrate of composition near CH₄·6.1H₂O (± 0.1 H₂O), which is the expected equilibrium stoichiometry for this compound at approximately 25-30 MPa methane pressure (9, 10). The resulting samples are translucent, white, cohesive aggregates of uniformly fine, equant grains with 250 ± 50 μ m grain size. The samples contain 28-30% porosity after full reaction (9). This porosity is eliminated by externally pressurizing sealed samples while venting the pore space gas, which we discuss later.

The detailed P-T-t curves (Fig. 4) and analyses of recovered samples revealed unexpected aspects of the reaction process. Figure 4 shows that deviation of the P-T record from the CH₄ self-pressurization curve first occurs just above the expected melting T of H₂O ice, 271.5 K at 28 MPa. As time proceeds, the rate of P increase slows as the hydrate-forming reaction consumes CH₄ gas (9). X-ray diffraction patterns of samples from runs with maximum temperatures below the ice melting curve showed no evidence of hydrate, and no deflections were observed in the P records to indicate any significant CH₄ mass uptake. Lack of appreciable reaction of CH₄ with ice below the H₂O liquidus was expected, in light of earlier investigations (6, 8).

After approximately 45% ΔP_r , the reaction rate decreases markedly. Full reaction was found to be most readily achieved by continuing to warm the system to conditions approaching the hydrate dissociation curve and well above the metastable extension of the H₂O melting curve (Figs. 1 & 4). To determine the rate of conversion of ice to hydrate at these conditions of T and P as a function of time, a series of partial-reaction experiments were quenched at various points along the full reaction curve, and subsequently weighed and x-rayed to determine hydrate content (Fig. 4, runs A - E). These partial-reaction tests indicate that during the early stages of reaction up to values of roughly 0.5 ΔP_r , the slow rate of seed ice melting still "outpaces" hydrate formation, as there is less hydrate in the samples than would be predicted by ΔP_r [see (5) for further discussion]. After this period, the rate of hydrate formation essentially keeps pace with incipient melting for the remainder of the 8 hours needed for full reaction at these conditions.

Figure 4 shows that there are no P-T discontinuities in the fabrication records to indicate bulk melting of the seed ice in the sample molds, even though full reaction to form hydrate at these conditions requires about 8 hours at temperatures well above the H₂O melting curve. The positive slope of the P-T curve within a few degrees above 271.5 K shows that there is not immediate and full melting of the ice as it is warmed above its liquidus, and there is a period of several tens of minutes after crossing the liquidus before there is any substantial indication of either ice melting or hydrate forming. These observations point to the conclusion that a large fraction of the seed ice exists in a superheated state for the many hours needed for full hydrate conversion.

This conclusion was verified by control experiments using neon (Ne, a non-hydrate-forming gas) in place of CH₄ gas, under the same environmental conditions and in the same apparatus as the methane hydrate samples (Fig. 5). We have previously described these results (5) and briefly outline them here. The Ne experiments confirmed that rapid, wholesale melting of the H₂O ice during the heating phase and refreezing of ice during the cooling phase of the tests (Fig. 5A) occurs in our apparatus when ice is not in the presence of a hydrate-forming gas, and that the associated P-T anomalies are easily detected. The T measured by the Ne sample thermocouple lags the rising T in the surrounding alcohol bath during the time interval over which the pressure drops (Fig. 5B), a phenomenon that we attribute to the absorption of heat by the expected endothermic melting of ice. In comparison, the T records of CH₄ runs displayed no such thermal anomalies, indicating that rapid, wholesale melting did not occur (Fig. 5B) (12). A prominent refreezing P-T anomaly occurred during the cooling phase of the Ne runs, and no P offset was detected after returning to the starting temperature (Fig. 5A). Visual inspection and x-ray identification of the final, quenched samples from the Ne experiments showed that they consist of clear cylinders of H₂O ice in the bottom of the mold, and that the loosely fitting top disk had sunk to the bottom, indicating full melting. In contrast, fully reacted methane hydrate samples have uniformly fine-grained granular textures and no displacement of the top disk. The Ne control experiments thus demonstrate that all the indicators of ice melting expected in our apparatus are actually observed when a non-hydrate-forming gas is used in the place of methane. The lack of such indicators in the methane experiments implies that such melting does not occur when hydrate is forming at our fabrication conditions.

The apparent suppression of macroscopic ice melting during methane hydrate synthesis raises several important questions; namely, why is full reaction achieved only after many hours at temperatures well above the the H₂O ice melting point, and why is there no evidence for wholesale melting of unreacted seed ice during this time? Probably of greatest influence is the availability of fresh ice surfaces to nucleate hydrate formation. For hydrate formation from either water or ice, the formation rate greatly diminishes once a surface layer of hydrate has formed, and vigorous shaking or stirring to crack the hydrate encasement and re-ew CH₄ access to ice/water surfaces is needed in order to continue the formation process at appreciable rates (13). Hwang and colleagues (8),

however, grew methane hydrate on disks of melting ice to measure hydrate growth rates at constant temperatures under static conditions. They observed two stages of methane hydrate formation, an initial "nucleation" period during which the formation rate increased with time, followed by a "growth" period, during which the formation rate decayed with time until no more ice remained on the disks. Hydrate growth rates were shown not only to be determined by the rate of the supply of the hydrate-forming species to the growth surface, but also by the rate of removal of the exothermic heat of formation from the forming surface (14). They concluded that the onset of melting ice along exposed surfaces not only promoted hydrate formation by providing a "template" for the formation of hydrates, but moreover, provided a heat sink for absorbing the heat of formation during hydrate growth. Once a rind of hydrate has encased an ice grain, the most likely process of continued hydrate formation involves solid-state diffusion of methane gas through the hydrate shell to the ice core (8, 15).

Our observations are in accord with the interpretations of Hwang et al. (8), and additionally we conclude from our sample textures and run records that this surface layer of hydrate encasing each seed ice grain not only rate limits reaction in the grain interior, but also serves to shield the ice grain from nucleating melt by removing the existence of a free external ice surface. A similar superheating effect has been measured in gold-plated silver single crystals, and results suggest that either a free external surface or internal defects or dislocations are critical for melting to take place at the normal "thermodynamic" melting point (16). In our experiments, methane hydrate may be producing a similar effect by shielding the ice cores from nucleating melt and from establishing a liquid-solid H₂O interface, by rapid reaction of incipient melt nuclei with CH₄ gas to form hydrate. We note that our method of seed ice preparation produces grains with few internal grain boundaries, and additionally, the ice grains are likely to anneal at the warm temperatures during fabrication, thus removing many of the internal defects for melt to nucleate on.

SOLID-STATE DEFORMATION TESTING & RESULTS

The strengths of methane hydrate specimens made by the above techniques were measured in constant-strain-rate tests in compression, at conditions ranging from T= 140 to 200 K, confining pressure (P_c) = 50 to 100 MPa, and strain rates ($\dot{\epsilon}$) = 3.5×10^{-4} to 10^{-6} s^{-1} (Table 1).

The testing apparatus is a 0.6 GPa gas deformation apparatus outfitted for cryogenic use, in which N₂ or He gas provides the P_c medium (17, 18) (Fig. 6). The thin, soft, indium jackets in which the samples were grown serve to encapsulate them during testing to exclude the P_c medium. Sample interiors were vented to room conditions by means of small-diameter tubing to allow initial compaction to eliminate porosity. The pressurized column within the apparatus consists of an internal force gauge, the jacketed sample, and a moving piston that compresses the sample axially against the internal force gauge at a fixed selected displacement rate (\dot{u}). Elastic distortion of the force gauge is measured outside the vessel and changes only with P_c and with the differential load that the piston exerts on the sample. In these experiments, differential force (F) and piston displacement (u) are recorded, corrected for changes from initial cross-sectional area and length (A_0, L_0) to instantaneous values (A, L), and converted to differential stress (σ), axial shortening strain (ϵ) and strain rate ($\dot{\epsilon}$) by the relationships: $\epsilon = u/L_0$; $\dot{\epsilon} = \dot{u}/L$; $A \cdot L = A_0 \cdot L_0$; $\sigma = F/A$. The force-time record (which we convert to stress-strain, as in Fig. 7B) usually reveals a transient response followed by a strength that ceases evolving with time, when various processes of work hardening and recovery have reached a steady-state condition.

Samples were subjected to a hydrostatic pressurization and compaction sequence at 170 K, prior to deformation. During this procedure, P_c was slowly "stepped" up to 100 MPa in increments of about 20 MPa. Following each P step, the piston was advanced to touch and square the bottom of the sample, then advanced just sufficiently to lightly compress the sample in order to compact it with minimal plastic deformation. Six of the samples were compacted using the internal vent line to eliminate the pore-space gas, and two of the samples were compacted without the venting capability. One sample (run 366, Table 1) was examined after compaction in the undeformed state. Volumetric measurements showed that virtually all porosity was eliminated, and that a cylindrical shape was largely maintained with only minor distortion of the sample. X-ray analysis showed evidence of a small fraction of H₂O ice in the sample ($\approx 7 \pm 3\%$), likely due to a disproportionation of hydrate as increasing P effects a stoichiometric change from CH₄·6.1H₂O to CH₄·5.8H₂O (10).

A suite of seven hydrostatically-compacted samples of methane hydrate were then tested by the methods described above and at the conditions shown in Table 1. Samples displayed measurably different steady-state strengths than H₂O ice, and results are summarized in Figure 7A. Moreover, the characteristics of transient deformation are markedly different. A typical stress-strain curve for methane hydrate is shown in Figure 7B; whereas H₂O ice ordinarily exhibits a strength maximum before leveling off to steady flow stress, usually within the first 5 - 10% of strain, methane hydrate exhibits monotonic work hardening (or strain hardening) that continues over more than 15% strain. This hardening effect persists to an extreme degree not only relative to other ices, but to most metals and ceramics as well.

Comparison of pre- and post-deformation x-ray diffraction analyses shows that samples underwent further structural changes while deforming within the nominal hydrate stability field. All deformed samples showed a significant volume fraction of ice in their final x-ray patterns (25% \pm 10%, Fig. 4B) compared with virtually no ice in their pre-test x-ray patterns (<3%, Fig. 4A), and also showed larger fractions of ice than detected in the pressurized-only sample (run 366). It is possible, however, that either heterogeneous ice precipitation or deformation-enhanced textural and grain size changes in the precipitated ice increased the apparent ice peak intensities. No peaks were observed in post-deformation x-ray patterns to indicate growth of any other new phase besides ice and structure I hydrate. We note that the two non-vented samples (281 & 282), showed equally large fractions of ice in their post-deformation x-ray patterns as the vented samples. After first detecting this apparent solid-state disproportionation of the hydrate, a gas collection system was attached to the vent line for two of the runs to observe and collect possible CH₄ gas evolving during deformation. The only gas that appeared from the vent, however, was that squeezed from the pores

during initial pressurization before deformation. No gas evolved from the system during any portion of deformation testing or subsequent unloading. While collapse of the hydrate structure could occur if as-molded material were strongly nonstoichiometric and contained significant lattice vacancies, this is unlikely as we measured nearly full uptake of CH₄ gas into the as-molded material. Double occupancy in lattice cages also seems unlikely as a possible explanation due to special considerations. We therefore conclude that at the deformation conditions of this study, methane hydrate appears to undergo a form of stress-enhanced exsolution and/or precipitation process within its nominal stability field. Precipitating H₂O ice may likely be causing a dispersion hardening process during hydrate deformation, a process that will be targeted in further studies.

SUMMARY

Methane hydrate displays exceptional characteristics that merit further investigation into the nature and behavior of this important compound. In the course of establishing optimal growth parameters for synthesizing hydrate samples suitable for rheological testing, we demonstrated that under conditions favorable to hydrate formation, the rate of H₂O ice melting may be suppressed to allow short-lived superheating of ice to temperatures well above its melting point. Deformation tests showed that not only does methane hydrate have a measurably different rheology than H₂O ice, but that it also undergoes extensive work hardening accompanied by a process of solid-state disproportionation during deformation at conditions well within its equilibrium stability field. Such unexpected consequences of methane hydrate formation and deformation may affect the physical, mechanical, and geochemical properties of hydrate-bearing sediments in ways not previously appreciated. In particular, hydrate instability under nonhydrostatic stress may affect environments such as those underlying continental shelves or in associated accretionary prisms prone to regional tectonic influences, where the presence of hydrates influences the strength, stability, porosity, pore-fluid composition, and migration pathways of hydrate-cemented sediments.

REFERENCES & NOTES

1. Natural gas hydrates belong to either of two crystal structures; methane hydrate (CH₄·6H₂O) is a structure I hydrate (1.2 nm cubic unit cell, space group *Pm3n*), constructed from 46 H₂O molecules and eight cavities available for CH₄ gas molecules.
2. E. Sloan, *Clathrate Hydrates of Natural Gases*, Marcel Dekker, Inc., New York, 641 p., 1990.
3. K. Kvenvolden, *Chemical Geology*, **71**, 41-51, 1988.
4. Because hydrates concentrate methane by a factor of 170 with respect to STP gas and as little as 10% of the recovered energy is required for dissociation, hydrate reservoirs are considered a substantial future energy resource; it has been estimated that the total amount of gas in this solid form may surpass the energy content of the total fossil fuel reserves by as much as a factor of two (2), (3), also Claypool, G.E., and I. R. Kaplan, in: Kaplan, I. R., (ed), *Natural Gases in Marine Sediments*, Plenum Press, New York, 99-139, 1974).
5. L. Stern, S. Kirby, and W. Durham, *Science*, **273**, 1843-1848, 1996.
6. R. Barrer and D. Ruzicka, *Trans. Faraday Soc.*, **58**, 2253, 1962; R. Barrer and A. Edge, *Proc. Roy. Soc. (London)*, **A300**, 1, 1967; B. Falabella and M. Vanpee *Ind. Eng. Chem. Fund.*, **13**, 228, 1974; K. Aoyogi, K. Song, R. Kobayashi, E. Sloan, and P. Dharmawardhana, *Gas Processors Assn. Research Report No. 45*, Tulsa, OK, 1980; see Sloan (2) for full review of fabrication techniques.
7. Hwang et al (8) noted that for hydrate formation from melting ice, higher gas P yields higher formation rates. Makogon (15) had earlier suggested that as hydrate formation is an interfacial process, high concentrations of hydrate-forming species are required at the interface.
8. Hwang, M.J., D.A. Wright, A. Kapur, and G. D. Holder, *J. Inclusion Phenom.*, **8**, 103-116, 1990.
9. The volume of an empty structure I hydrate lattice is 16% greater than the equivalent mass of ice I [the empty structure I lattice has a density of 0.78, and stoichiometric methane hydrate has a density near ice (0.90 vs 0.92 for ice)], but there is a large ΔV associated with hydrate formation due to the volume reduction of the gas phase into the hydrate structure. Here, we start with 26 g of seed ice, and the actual molar reaction is: 1.4H₂O + 0.23 CH₄ (g) \rightarrow 0.23(CH₄·6.1H₂O). The 3.8 g of CH₄ uptake measured after sample synthesis confirms this hydrate stoichiometry and is consistent with (10). Independent measurement of CH₄ collected from a dissociating sample also verified this stoichiometry (K. Kvenvolden and T. Lorenson, personal communication). While ΔV of the reaction is nearly 21%, we only measure a 6.4% associated drop from the starting P due to the large volume of the combined reservoir plus sample chamber.
10. Gas hydrate number *n* varies with P; increasing P maximizes guest-molecule site occupancy. At sample synthesis conditions (~28 MPa) *n* for methane hydrate should be 6.1 \pm 0.1, and at 100 MPa *n* = 5.85 \pm 0.05 (S. Saito, D. Marshall, and R. Kobayashi, *AICE J.*, **10**, 734, 1964; also see (11), p.54.)
11. *Handbook of gas hydrate properties and occurrence*. U.S. DOE Publication DOE/MC/19239-1546, 234p., 1983.
12. The reaction CH₄ (g) + 6H₂O (ice) \rightarrow CH₄·6H₂O liberates a small amount of latent heat ($\approx 20 \pm 5$ kJ/mol at 273 K and a CH₄ P of 28 MPa, determined from the Clapeyron slope (T. Makogon and E. Sloan, *J. Chem. and Eng. Data* **39**, 2, 351-353, 1994), the measured enthalpy of formation at standard conditions (Y. Handa, *Chem Thermodynamics* **18**, 915-921, 1986), ΔV_f (9), and its variation with P (11).) This heat is not reflected as a T anomaly (Fig. 5B), evidently because reaction occurs over a period of 8 hours and such heat would be small compared with the exchange of heat of the sample with its surroundings by conduction. (The standard enthalpy for melting of ice is -6.01 kJ/mol, or -36 kJ/6 moles for comparison with the hydrate-forming reaction).
13. The importance of vigorous agitation to renew ice/water surfaces for hydrate formation was established by Villard (P. Villard, *Compt. Rend.*, **106**, 1602, 1888) and is also discussed by Sloan (2) and Hwang et al (8).
14. Hwang et al. (8) note that as hydrate formation is an exothermic process, the heat released by the phase change increases the T at the formation interface. This effect is greater for hydrate formation from liquid water than from ice since the heat of formation is partially absorbed by the melting ice.
15. Y. Makogon, *Hydrates of Natural Gases*, W.H. Cielewicz Translation, PennWell Publishing, Tulsa OK, 1981.
16. J. Daeges, H. Gleiter, and J. Perepezko, *Phys. Lett.*, **119A**, 79, 1986. See also: S. Phillpot, J. Lutsko, D. Wolf, and S. Yip, *Phys. Rev. B*, **40** (5), 283-2840, 1989, and S. Phillpot, S. Yip, and D. Wolf, *Computers in Physics*, **3**, 20-31, 1989, for further discussion of results.
17. H. Heard, W. Durham, C. Boro, and S. Kirby, in *The Brittle-Ductile Transition in Rocks, Geophysical Monograph* **56**, ed. by A. G. Dube et al., American Geophysical Union, Washington, D. C., 225-228, 1990.
18. W. Durham, S. Kirby, and L. Stern, *J. Geophys. Res.* **97**, E12, 20,883-20,897, 1992; also S. Kirby, W. Durham, M. Beeman, H. Heard, and M. Daley, *J. Phys.*, **48**, suppl., 227-232, 1987.
19. This work was supported under NASA order W-18927, and was performed in part under the auspices of the USGS and in part by the U. S. DOE by the Lawrence Livermore National Laboratory under contract W-7405-ENG-48.

Table 1. Mechanical test conditions and results.

Run# (step)	T (K)	P _c (MPa)	$\dot{\epsilon}$ (s ⁻¹)	ϵ_t	σ_y (MPa)	σ_{SS} (MPa)	Comments
281	160	50	3.5×10^{-4}	0.125	---	>85	Strain hardening.
2	160	50	3.5×10^{-6}	0.150	---	60	Strain hardening.
3	160	50	3.5×10^{-4}	0.160	100	---	Brittle failure. $\approx 25\%$ H ₂ O ice ^b .
282	140	50	3.5×10^{-6}	---	71	---	Failure, multiple events.
2	140	50	3.5×10^{-4}	0.160	94	---	Failure, multiple events. $\approx 25\%$ ice ^b .
366	168	100	---	---	---	---	Pressurization & compaction only;
367	185	100	3.5×10^{-5}	0.138	---	71	Strain hardening at 10^{-5} step.
2	185	100	3.5×10^{-4}	0.215	96	90	$\approx 30\%$ ice post-deformation.
368	168	100	3.5×10^{-5}	0.185	---	102	Strain hardening. 25% ice ^b .
369	168	100	3.5×10^{-5}	0.16	---	100	Identical run as 368 ^d . No evolved CH ₄ gas.
370	200	100	3.5×10^{-5}	0.120	---	62	Strain hardening at 10^{-5} . No evolved gas ^d .
2	200	100	3.5×10^{-4}	0.230	85	80	$\approx 30\%$ ice post-deformation.

^a P_c is confining pressure gas medium; ϵ_t is total strain; σ_y is yield strength; σ_{SS} is steady-state strength.

^b Post-deformation, determined by x-ray diffraction.

^c Samples 367, 368, 369, & 370 all underwent identical pressurization and compaction as 366 prior to testing.

^d Runs 369 & 370 had a gas collection system attached throughout testing to detect evolved CH₄ gas.

Figure 1: Phase diagram for the CH₄-H₂O system. Shaded region shows field of methane hydrate stability. At low pressures or high temperatures, methane hydrate dissociates to H₂O (ice or liquid) plus CH₄ gas. The metastable extension of the H₂O melting curve is shown by the grey curve. Dashed lines trace the sample fabrication reaction path (described in text.) Solid squares show pressure and temperature conditions of deformation tests (note change in pressure scale on y-axis from linear to log scale.) CH₄ cp designates methane critical point.

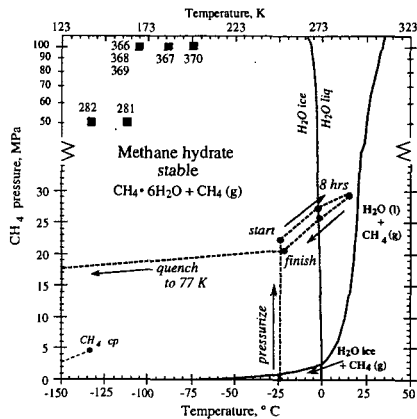


Figure 2: Apparatus for fabricating cylindrical test specimens of methane hydrate from CH₄ gas and melting ice. The sample assembly is housed in a freezer at 250 K, and consists of two steel vessels immersed in an ethyl alcohol bath. One vessel stores a reservoir of cold, pressurized CH₄ gas at 35 MPa and 250 K, and the second contains the sample mold with pre-jacketed and pre-evacuated H₂O "seed" ice. Two-way valves allow isolation of any component of the assembly, and a vacuum pump connected to the sample chamber permits evacuation of the system. The sample chamber is warmed by a hot plate situated beneath the alcohol bath and controlled remotely with a variable autotransformer. Temperature is monitored by thermocouples enplaced in the base of the sample mold and in the bath, and pressure is measured by the gauge and transducer, as shown. Procedures promoting methane hydrate crystallization are described in the text.

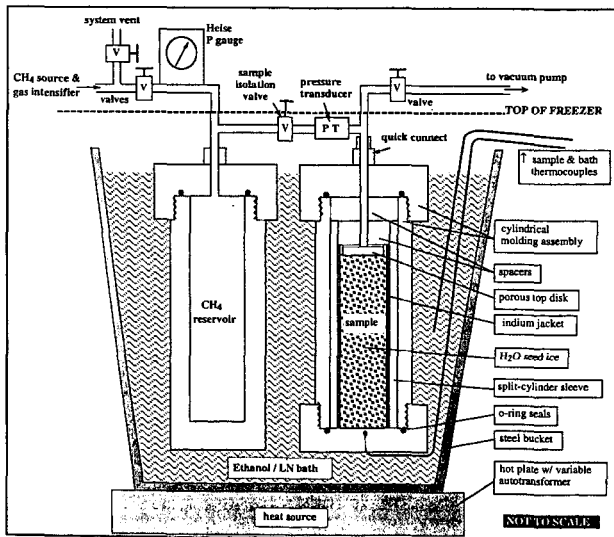


Figure 3:

X-ray powder diffraction patterns for methane hydrate as grown (A) and after mechanical testing (B). Methane hydrate deformed under nonhydrostatic stress undergoes a partial solid-state disproportionation, as evidenced by H₂O ice peaks (dotted lines) found in post-deformation x-ray diffraction patterns.

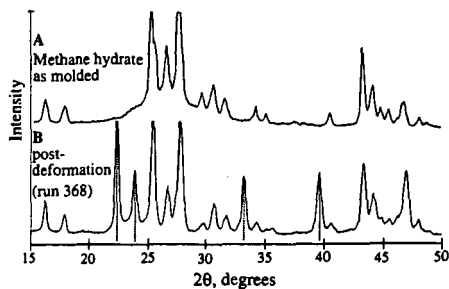


Figure 4:

(A) Temperature-pressure profile of sample fabrication conditions promoting the hydrate-forming reaction: $\text{CH}_4(\text{g}) + \text{H}_2\text{O}(\text{ice}) \rightarrow \text{CH}_4 \cdot 6\text{H}_2\text{O}$. Warming the ice + gas mixture above the H₂O solidus (dot-dashed line, point A) initiates reaction. Increasing temperature slowly to 289 K, over an 8 hour span, accelerates full reaction. Complete reaction in our apparatus is marked by a 1.8 MPa pressure drop (ΔP_f) from start to finish. Squares A-E correspond to individual samples that were quenched at specific intervals during hydrate formation to determine hydrate content as a function of ΔP_f and time.

(B) Temperature-time profile during hydrate formation. Hydrate content (vol.%) of samples A-E given on top scale bar, and show how the rate of hydrate formation decays with time under static growth conditions.

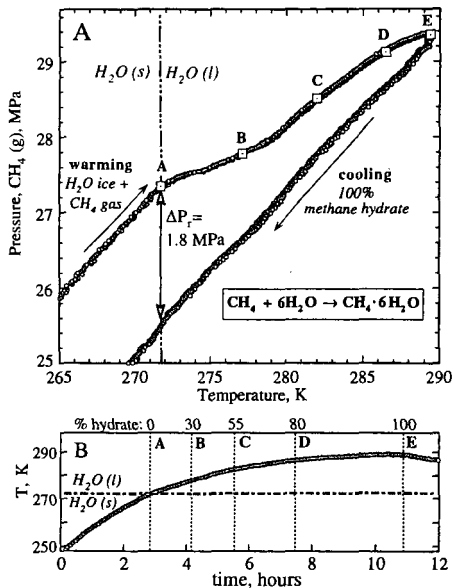


Figure 5:

(A) Temperature-pressure record of neon gas + H₂O ice experiment demonstrates full melting and refreezing of H₂O ice near its solidus when in the presence of non-hydrate-forming gas. The Ne + ice run shows no net pressure drop associated with melting and refreezing, so start-finish conditions are coincident.

(B) Detail of temperature-time history of Ne (g) + H₂O ice in the region of ice melting, showing the lag of the sample temperature compared to the bath temperature associated with the absorption of heat by the endothermic melting of ice. No such effect is displayed by the thermal history of the methane hydrate experiment, also shown (grey open circles).

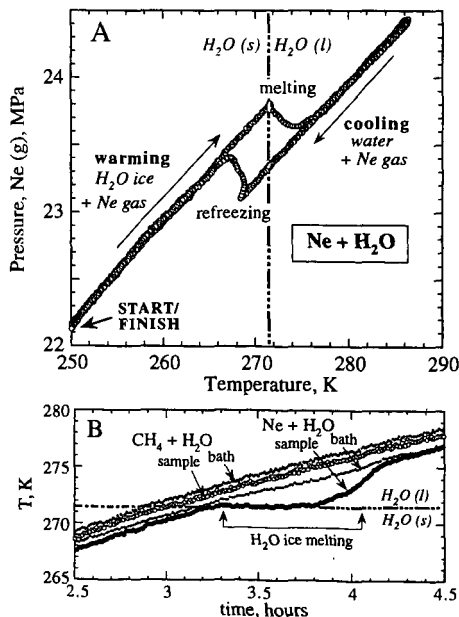


Figure 6:

Schematic of triaxial gas deformation apparatus set up for methane hydrate testing at cryogenic temperatures. The indium-jacketed sample sits within a cylindrical pressure vessel in which N_2 or He gas provides the confining medium. A sliding piston moves through dynamic seals from below to impose constant axial shortening. Samples are mounted on to a "venting" internal force gauge permitting sample communication with room conditions and allowing initial hydrostatic pressurization to eliminate residual porosity prior to deformation. The gas collection system (shown at top) was attached during several tests to monitor possible loss of methane gas during deformation.

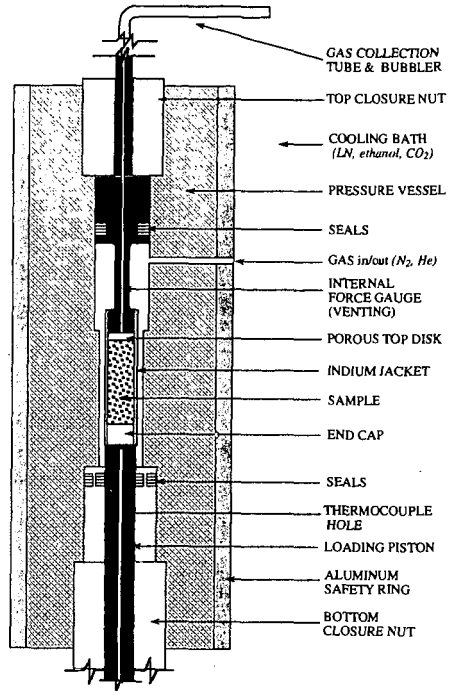


Figure 7:

(A) Strength measurements of methane hydrate show that it has measurably different strength than H_2O ice. Ice flow constants are from (18). Methane hydrate data points with arrows indicate faulting behavior.

(B) Stress-strain curves of deformed methane hydrate (run 368) compared to "standard" polycrystalline H_2O ice. While the strengths of the two compounds are comparable, methane hydrate undergoes systematic strain hardening to an extreme degree (over 18% strain) while H_2O ice typically displays an ultimate yield strength followed by relaxation to steady state behavior.

